BB

SW 9403

PREPRINT

TASCC-P-93-17

tascc

Recoil Distance Lifetime Measurements of States in the Oblate Dipole Bands of ^{197,198}Pb

R.M. Clark[1], R. Wadsworth[1], H.R. Andrews[2], C.W. Beausang[3], M. Bergstrom[3], S. Clark[3], E. Dragulescu[1+], T. Drake[4], P.J. Dagnall[3], A. Galindo-Uribarri[2], G. Hackman[5], I.M. Hibbert[1], K. Hauschild[1], V.P. Janzen[2], P.M. Jones[3], R.W. MacLeod[2], S.M. Mullins[5], E.S. Paul[3], D.C. Radford[2], A. Semple[3], J.F. Sharpey-Schafer[3], J. Simpson[6], D. Ward[2], G. Zwartz[4]

[1]Department of Physics, University of York, Heslington, York, Y01 5DD, UK
[2]AECL Research, Chalk River Laboratories, Chalk River, ON K0J 1J0, Canada
[3]Oliver Lodge Laboratory, University of Liverpool, Liverpool, L69 3BX, UK
[4]Department of Physics, University of Toronto, Toronto, ON M5S 1A7, Canada
[5]Department of Physics and Astronomy, McMaster University, Hamilton, ON L8S 4M1, Canada
[6]Nuclear Structure Facility, Daresbury Laboratory, Daresbury, Warrington, WA4 4AD, UK

[+] Permanent address: Institute for Atomic Physics, Tandem Laboratory, Bucharest-Magurele R-79600, Romania

Submitted to Phys. Rev. C

NOTICE

Physical Sciences
Chalk River Laboratories
Chalk River, ON K0J 1J0, Canada

1993 December

Recoil Distance Lifetime Measurements of States in the Oblate Dipole Bands of ^{197,198}Pb

R.M.Clark[1], R.Wadsworth[1], H.R.Andrews[2], C.W.Beausang[3], M.Bergstrom[3], S.Clark[3], E.Dragulescu[1†], T.Drake[4], P.J.Dagnall[3], A.Galindo–Uribarri[2], G.Hackman[5], I.M.Hibbert[1], K.Hauschild[1], V.P.Janzen[2], P.M.Jones[3], R.W.MacLeod[2], S.M.Mullins[5], E.S.Paul[3], D.C.Radford[2], A.Semple[3], J.F.Sharpey-Schafer[3], J.Simpson[6], D.Ward[2], G.Zwartz[4]

[1] Department of Physics, University of York, Heslington, York, Y01 5DD, UK.
[2] AECL Research, Chalk River Laboratories, Chalk River, ON KOJ 1J0, Canada.
[3] Oliver Lodge Laboratory, University of Liverpool, Liverpool, L69 3BX, UK.
[4] Department of Physics, University of Toronto, Toronto, ON M5S 1A7, Canada.
[5] Department of Physics and Astronomy, McMaster University, Hamilton, ON L8S 4M1, Canada.
[6] Nuclear Structure Facility, Daresbury Laboratory, Daresbury, Warrington, WA4 4AD, UK.

Abstract

Lifetimes of states in four of the oblate dipole bands in ^{197,198}Pb have been measured with the recoil–distance technique. Using all the available data on lifetimes and branching ratios, and assuming pure magnetic dipole transitions, we deduce reduced transition probabilities. The results are consistent with weakly oblate collective structures involving high–K proton configurations coupled to rotationally aligned neutrons. Comparisons are made to the theoretical estimates of the Dönau and Frauendorf semi–classical model and the Tilted Axis Cranking (TAC) model.

† Permanent address: Institute for Atomic Physics, Tandem Laboratory, Bucharest–Magurele R–79600, Romania.

1 Introduction

The recent observation of cascading sequences of magnetic dipole transitions in the neutron–deficient Pb [1–10] and Bi [11, 12] nuclei has prompted a great deal of interest. These structures have generally been interpreted as weakly oblate (β_2 ~–0.05 to –0.15) high–K proton configurations coupled to rotationally aligned neutrons. The assignment of configurations to each band has so far been based on considerations, such as:

- Regularity of energy spacing, ΔE_γ, between successive transitions.
- Lower limits to the $B(M1)/B(E2)$ ratios.
- Behaviour of the dynamic moments of inertia, $\Im^{(2)}$, as functions of rotational frequency, ω.
- Identical transition energies (to within ~3 keV) of different bands in different nuclei.

In order to provide further evidence for configuration assignments accurate lifetime measurements for states within the bands have to be made. These can then be related to theoretical predictions of the magnetic dipole (M1) transition rates for the various possible configurations. If accurate branching ratios are known for the crossover decays, the E2 transition rate can be used to deduce the quadrupole moments of the structures. The first Doppler Shift Attenuation Method (DSAM) lifetime measurements have recently been reported for two of the bands in ^{198}Pb [7] and for the strong regular band in ^{197}Pb [10]. These support the oblate collective interpretation but do not uniquely specify a configuration for each band.

In this paper we present lifetime measurements of several states in each of four different dipole sequences, two in ^{197}Pb and two in ^{198}Pb. The results were obtained from a recoil distance (RDM) experiment with the 8pi spectrometer, which was specifically aimed at measuring the lifetimes of states near to the bandheads of each structure, complementing the previous DSAM measurements. Accurate branching ratios, required to deduce B(M1) and B(E2) transition rates, were found by the analysis of high–fold, high–statistics data taken with the EUROGAM spectrometer. The deduced M1 transition rates are compared with theoretical estimates of the Dönau and Frauendorf semi–classical model [13] and the Tilted Axis Cranking (TAC) model [14].

2 Experimental Work

An experiment was performed at the Tandem Accelerator Superconducting Cyclotron (TASCC) facility at Chalk River. The reaction used to populate high–spin states in ^{197,198}Pb was ^{176}Yb(^{26}Mg,xn)$^{202-x}$Pb at a beam energy of 125 MeV.

Gamma–rays were detected with the 8π–spectrometer [15] which consists of a 70–element bismuth germanate (BGO) ball and an array of 20 high-resolution Compton–suppressed Ge detectors. A ring of five Ge detectors is situated at each of the polar angles, $\pm$79° and $\pm$37° relative to the beam axis. The data comprised the energy deposited in each Ge detector, the sum–energy, H, and fold, K, recorded by the BGO ball, and the timing of the Ge–event with respect to the triggering of the BGO ball. A hardware fold condition of K>4 was imposed before the data was recorded on magnetic tape.

Lifetimes were measured with a standard recoil distance Doppler–shift method [16, 17]. A precision plunger, designed and built at the Chalk River Laboratories, was used. The target consisted of an 800 μgcm^{-2} ^{176}Yb foil mounted on a 1 mgcm^{-2} Au frontal support, which degraded the effective beam energy to 121 MeV. The stopper was a 4.8mgcm^{-2} gold foil. The two foils formed a parallel–plate capacitor. Initial alignment was achieved through an computer–controlled tilt adjustment technique which maximized the capacitance. The separation was continually monitored during the experiment by a capacitive method [16]. Data were recorded at 0.0, 5.5, 7.0, 8.6, 11.8, 15.0, 23.0 and 5000 μm. The nominal separation was maintained within an accuracy of 0.2 μm for points in the range 0.0 to 23.0 μm. Approximately 10^7 γ–γ–BGO events were recorded at each distance. The average recoil velocity was determined to be 1.13$\pm$0.05% of the velocity of light from the relative separation of shifted and unshifted components of γ–ray lines.

The γ–γ coincidence data were sorted off–line into matrices which contained events from detectors at $\pm$79° (y–axis) against events in detectors at +37° or −37° (x–axis). In addition, software fold conditions of 5≤K<14 and K≥11 were used to enhance preferentially ^{197}Pb and ^{198}Pb contributions to the γ–γ matrix, respectively. Thus, a total of four matrices were sorted at each distance.

To determine accurately the very weak E2 branching ratios another experiment was performed. High–spin states in ^{197,198}Pb were populated by the ^{186}W(^{18}O,xn) reaction at a beam energy of 113 MeV. The beam, which was provided by the 20 MV Tandem Van de Graaff accelerator at the Nuclear Structure Facility, Daresbury Laboratory, was incident upon a target consisting of three stacked ^{186}W foils, on thin carbon backings, with a total thickness of 600μgcm^{-2}. Gamma rays were detected with the EUROGAM spectrometer [18] which comprised 43 high–volume Compton–suppressed Ge detectors. Approximately 4×10^8 events with an unsuppressed fold of ≥5 were recorded. The data were sorted into a two–dimensional γ_1–γ_2 matrix which contained events with a suppressed fold of 4 and higher unpacked into all possible γ–γ doubles combinations. The resulting matrix contained $\sim2\times10^9$ events.

3 Recoil Distance Method Data Analysis

Detailed descriptions of typical RDM analyses and the limitations encountered can be found in the literature, e.g. [17]. A software analysis package developed at Chalk River was used to analyse the data. Energy gates were set on the $\pm$79° detectors where the Doppler shift is small. Side–feeding corrections were eliminated, where possible, by gates set above the state of interest. It should be noted that the population intensities of all the bands are known from previous studies [3, 4, 6, 7]. It is clear from these data that there is little or no side–feeding into the states for which lifetime measurements have been made. The intensities of the shifted, I_S, and unshifted, I_U, components of a γ–ray transition could then be measured in the resultant $\pm$37° sum–gated spectra. The relative positions and widths of the peaks were fixed for all the spectra at each distance. The spectra formed at each distance were normalized to the intensity of either the 929 keV ($14^+ \rightarrow 12^+$) transition in ^{198}Pb or the 1006 keV ($17/2^+ \rightarrow 13/2^+$) transition in ^{197}Pb. Examples of γ–ray spectra are presented in Fig. 1 while Fig. 2 shows some fitted decay curves.

It is necessary to model the cascade above the state of interest. This was done by a numerical solution of the Bateman equations [19] for the sequence of states which form the cascade. These equations describe the population of the states as a function of time. It is necessary to introduce lifetime estimates of levels in the cascade into the model. For the two bands in ^{198}Pb and the regular band in ^{197}Pb this was done with the DSAM results [7, 10]. Three levels with known lifetimes were used to approximate the cascade above the state of interest. It was found empirically that adding more levels to the model of the cascade made little difference to the extracted lifetime. For the irregular sequence in ^{197}Pb this method was not applicable since lifetimes of states in the sequence had not been measured prior to the present investigation. Instead, the highest state for which a depopulation time could be extracted was used as a model of the entire cascade up to that point. The intrinsic lifetimes of states lower in the cascade could then be extracted. A comparison of the two approaches indicated that the second method often estimated the intrinsic lifetime of the state directly beneath it to be 10 to 20% greater than when determined with the first method. The derived lifetime of a state depends upon the accuracy of the estimates for the lifetimes of the immediate precursors. This was taken into account in assessing the final uncertainties.

4 Results

The lifetimes of sixteen levels from four bands (two in ^{197}Pb and two in ^{198}Pb) have been measured. In addition, estimates of the lifetimes of several states beneath both the bands in ^{198}Pb have been made. In order to aid the discussion, the labelling scheme given in [6] will be used for the structures in ^{198}Pb. The two bands in ^{197}Pb for which lifetime measurements were possible are those described in [3, 4]. Partial level schemes showing each of the structures are presented in Figs. 3 and 4.

Tables 1 and 2 summarize the results obtained in the present work together with the results of the previous DSAM measurements for the bands in ^{198}Pb [7]. Table 1 also contains the corresponding B(M1) values which have been deduced from the formula [20]:

$$B(M1) = \frac{0.03183 B_\gamma}{E_\gamma^3 \tau (1 + \alpha_{TOT})} \qquad [Wu] \tag{1}$$

E_γ is the transition energy in MeV and τ is the mean intrinsic lifetime of the state in ps. The transitions were assumed to be of pure M1 character. This assumption is based on the results of previous studies which generally found very small negative mixing ratios. Values of the internal conversion coefficients were taken from [21]. The branching ratios, B_γ, were taken from the EUROGAM data and are given in Table 1. This is the first time that several associated E2–quadrupole transitions have been firmly identified in this type of structure. The B(M1)/B(E2) ratios measured are presented in Table 2.

A few general points need to be made. Firstly, structure A in ^{198}Pb needs alteration from the ordering given in [6, 7] (see Fig. 3). From the measured decay curves we find the depopulation times, t, to be such that $t_{336} < t_{429} < t_{228}$ (5.4(16), 6.2(19), 7.8(19) ps, respectively). This suggests that the 336 keV transition must be above the 429 keV γ–ray, which in turn must be above the 228 keV transition. Assuming that this ordering is correct then the extracted intrinsic lifetimes are those quoted in Table 1. The parallel path (see Fig. 3) is too weak to extract any lifetimes.

The lower limits of the lifetimes of three transitions in structure B in ^{198}Pb are also given in Table 1. We found them by observing at which distance the transitions first began to shift. For the 264 and 532 keV γ–rays a noticable shift occurred for d≥11.8 μm. For the 322 keV transition a shift was only seen for d≥23 μm. These observations support the ordering given in [6].

The state that decays via the 228 keV γ–ray was the highest state for which a depopulation time was measured (see Fig. 4). Lifetimes of states below this were estimated. The decay curves confirmed the ordering of states in this sequence as given in [4] with the exception of the 433 and 127 keV transitions. These two previously reported members of the cascade were found to have depopulation times much longer than the measurable range covered by the experiment (i.e., the γ–rays did not shift until d>23μm), while the lowest transition (152 keV) of the band did have an extractable lifetime. Therefore, we conclude that these two transitions are not members of the band but lie somewhere beneath it.

5 Discussion

In the following discussion it is convenient to use the labelling convention developed in [6] whereby the (unpaired) neutron occupations are given relative to the oblate N=120 subshell closure. The configurations that have been previously proposed for the four structures [6] are presented in Table 3. Different configurations will generally have different B(M1) values associated with them. By comparing the values in Table 1 it is clear that the B(M1) rates for band 1 in ^{198}Pb and the regular band of ^{197}Pb are similar. They are greater on average than the values for band 3 in ^{198}Pb which in turn are greater than the B(M1) values for the irregular sequence in ^{197}Pb. The situation is illustrated in Fig. 5. It may be concluded from these observations that at least three different configurations must be involved in these structures. This is in accordance with the configuration assignments show in Table 3.

The $(h_{9/2}\otimes i_{13/2})_{K=11}$ proton configuration is predicted to be the most deformed of the structures and it is expected to have larger B(M1) transition rates than either the $(h_{9/2})^2_{K=8}$, or $(h_{9/2}\otimes s^{-1}_{1/2})_{K=5}$ configurations (assuming similar numbers of $i_{13/2}$ (N=6) neutrons (or neutron holes), see later). Indeed, the highest measured B(M1) values are found for the two structures that are associated with this proton configuration. Furthermore, associated E2–crossover transitions for states with known lifetimes can be seen for three of the four dipole sequences. From the measured branching ratios, B_γ, we have estimated B(E2) transition rates via the formula, [20]:

$$B(E2) = \frac{0.08156 B_\gamma}{E_\gamma^5 \tau (1+\alpha_{TOT})} \qquad [e^2b^2] \qquad (2)$$

where E_γ is the energy of the E2 transition in MeV and τ is the lifetime of the state in ps. The E2 internal conversion was neglected. From the B(E2) it is possible to find the intrinsic quadrupole moment since, in a rigid rotor model:

$$B(E2) = \frac{5}{16\pi} Q_0^2 \langle I + 2K20|IK\rangle \tag{3}$$

where Q_0 is the intrinsic quadrupole moment in eb. The Clebsch–Gordan coefficient varies only by ~10% over the range of plausible K–values when I>20. The intrinsic quadrupole moment of the irregular band in ^{197}Pb was found to be Q_0=1.0(1) eb while that of band 1 in ^{198}Pb was Q_0=2.0(2) eb. The intrinsic quadrupole moment for band 3 in ^{198}Pb was found to lie at an intermediate value of around 1.3(2) eb. Table 4 summarizes the B(E2) estimates for the bands and also gives the deduced values of the intrinsic quadrupole moments, Q_0, and quadrupole deformations, β_2. The absolute values of the quadrupole deformations are somewhat smaller than predicted, β_2 ~0.03–0.08 (see Table 4). Note, that if the oblate shape becomes slightly triaxial (γ ~–70°), as predicted by TRS calculations [6], then the quoted β_2 values would increase by ~10–20%. There is consistency with the configuration assignments presented in Table 3 since the TRS calculations predict that the $(h_{9/2}\otimes s_{1/2}^{-1})_{K=5}$ proton configuration should have the lowest deformation (β_2 ~0.07) while the $(h_{9/2}\otimes i_{13/2})_{K=11}$ structure should have the largest deformation (β_2 ~–0.15). The deformation of the $(h_{9/2})^2_{K=8}$ configuration is between these two (β_2 ~–0.10).

Evidently there is good qualitative agreement between the results and the proposed configuration assignments presented in Table 3. For a more quantitative comparison absolute B(M1) transition probabilities need to be calculated within an appropriate theoretical framework. A simple approach is to apply the semi–classical Dönau and Frauendorf formula [13] which computes contributions to the B(M1) from both the deformation–aligned protons and rotationally aligned neutrons.The g–factor of the $i_{13/2}$ neutrons was taken as –0.18. The g–factors of the $(h_{9/2}\otimes i_{13/2})$, $(h_{9/2})^2$, and $(h_{9/2}\otimes s_{1/2}^{-1})$ proton configurations were taken as 1.02, 0.78, and 1.04, respectively. These were estimated from the Schmidt values. Note, the estimates are a possible source of error in the deduction of the B(M1) values. However, the measured g–factor for the I^π=11$^-$ isomer in ^{196}Pb is 0.96(8) [22], and the g–factor of the $\nu(i_{13/2}^2)_{12^+}$ state in ^{200}Pb is –0.16(1) [23], which indicate that our estimates are reasonable. Results for the different possible proton configurations, coupled to various numbers of $i_{13/2}$ (N=6) neutrons, are given in Table 5. The theoretical values overestimate the measured B(M1)'s by at least a factor of two, especially when one or more $i_{13/2}$ neutrons are involved. It should be noted that $i_{13/2}$ neutrons must be present in some configurations in order to explain the observed alignments [3–7]. The contribution of other alignable neutrons (N=5), occupying orbitals close to the Fermi surface (e.g $p_{3/2}$, $p_{1/2}$, $f_{5/2}$), will raise the calculated B(M1) estimates by ~10%.

Theoretical estimates of the B(M1;I→I–1)/B(E2;I→I–2) ratios were also found with the Dönau and Frauendorf formalism. For the $\pi(h_{9/2}\otimes i_{13/2})$ configuration coupled to three $i_{13/2}$ quasineutrons the B(M1)/B(E2) ratios were found to be $\geq 30(\mu_N/\mathrm{eb})^2$ over a wide spin range. For the $\pi(h_{9/2})^2$ and $\pi(h_{9/2}\otimes s_{1/2}^{-1})$ configurations, coupled to three $i_{13/2}$ quasineutrons, the ratios were found to be $\sim 10(\mu_N/\mathrm{eb})^2$ for I~20$\hbar$. These values are qualitatively consistent with the measured B(M1)/B(E2) ratios as given in Table 2.

The combination of high–spin protons and high–spin neutrons associated with these oblate dipole bands presents an unusual circumstance, possibly not described by the familiar coupling schemes of angular momentum. A new approach has been provided by Tilted Axis Cranking (TAC) [14]. This provides a semi-classical description of many-quasiparticle $\Delta I=1$ bands at high-spin. Enhanced M1 transitions arise naturally as a consequence of the breaking of signature symmetry.

A calculation of the B(M1) transition rates for the $\pi(h_{9/2}\otimes i_{13/2})\otimes\nu(6^{-x}5^{y})$ configurations in ^{198}Pb has recently been reported [14]. The neutron configurations were generated by excitations of the $i_{13/2}$ ABC quasineutron states and the negative parity state E (in Cranked Shell Model notation). The deformation was fixed at β_2=0.12 and γ=-60° (i.e. weakly oblate). A simple geometric picture arises whereby combinations of the protons with the $i_{13/2}$ neutrons gives rise to an equilibrium with the rotation axis (which is parallel to the total angular momentum vector, I) lying at ~45° relative to the symmetry axis. The total angular momentum vector is increased when the individual proton, $\mathbf{i}_\pi$, and neutron, $\mathbf{i}_\nu$, spins gradually tilt towards I. Fig. 6 schematically illustrates this situation.

Large B(M1) values are predicted to be $\simeq$1 Wu [14]. However, the calculations overestimate the experimental values by approximately a factor of two for both the AB and ABCE quasineutron configurations. In addition, the gradual alignment of the proton and neutron spins along the tilted rotation axis should push the B(M1) values down as the angular momentum increases [14] . This feature is not observed. Thus, a theoretical approach that gives accurate B(M1) values for the oblate dipole bands in the neutron deficient Pb nuclei is still required. One possible technique is full three-dimensional cranking, e.g. [24, 25, 26]. This method does not assume uniform rotation. Non-uniform rotation (wobbling) may possibly account for some of the observed features. Full solution of the 3D-cranking problem is much more complex than the TAC procedure.

It would be interesting to compare the predictions of the TAC model against measured B(M1) transition rates of $\Delta I=1$ bands in the A~130 region [27-30]. These sequences are generated in an analogous manner to the A~190 oblate dipole bands, but in this lighter-mass region high-K $h_{11/2}$ quasiprotons couple to alignable $h_{11/2}$ quasineutrons.

6 Summary

Lifetimes of sixteen states in four different dipole sequences of ^{197,198}Pb have been measured with the recoil-distance technique. Estimates of lifetimes have also been found for several states beneath the two bands in ^{198}Pb. In addition, several E2-crossover transitions associated with the bands have been seen for the first time in high-statistics data from the EUROGAM spectrometer. From accurate branching ratios and all the available lifetime data B(M1) and B(E2) transition probabilities were deduced. They were shown to be qualitatively consistent with previous configuration assignments of the structures as given in [6]. For each structure, the absolute B(M1) values, calculated either with the model of Dönau and Frauendorf or with the TAC semi-classical model, were found to be at least a factor of two too large.

Acknowledgements We would like to express our gratitude to Peter Dmytrenko, for his hard work in producing the high–quality target foils used in the experiment. We gratefully acknowledge several useful discussions with Professor Stefan Frauendorf on the TAC method. Thanks also go to Dr. Rhys Hughes, and collaborators, for providing us with data prior to its publication. This work was supported by AECL Research, and by grants from the UK Science and Engineering Research Council and the Natural Sciences and Engineering Research Council of Canada. Five of us (RMC, SC, PJD, PMJ, and AS) acknowledge receipt of UK SERC postgraduate studentships. We also wish to thank the crews and staff of the Chalk River TASCC facility and the Daresbury NSF. EUROGAM is jointly funded by the SERC and IN2P3.

References

[1] P.Dagnall, C.W.Beausang, P.Fallon, P.D.Forsyth, E.S.Paul, J.F.Sharpey-Schafer, P.J.Twin, I.Ali, D.M.Cullen, M.J.Joyce, G.Smith, R.Wadsworth, R.M.Clark, P.H.Regan, A.Astier, M.Meyer, N.Redon, J. Phys. G 19 (1993) 465

[2] J.R.Hughes, Y.Liang, R.V.F.Janssens, A.Kuhnert, I.Ahmad, I.G.Bearden, J.A.Becker, M.J.Brinkman, J.Burde, M.P.Carpenter, J.A.Cizewski, P.J.Daly, M.A.Deleplanque, R.M.Diamond, J.E.Draper, C.Duyar, B.Fornal, U.Garg, Z.W.Grabowski, E.A.Henry, W.Hesselink, N.Kalanter-Nayestanaki, W.H.Kelly, T.L.Khoo, T.Lauritsen, R.H.Mayer, D.Nissius, A.J.Plompen, J.R.B.Olivera, W.Reviol, E.Rubel, F.Soramel, F.S.Stephens, M.A.Stoyer, D.Vo, T.F.Wang, Phys. Rev. C 47 (1993) R1337

[3] R.M.Clark, R.Wadsworth, E.S.Paul, C.W.Beausang, I.Ali, A.Astier, D.M.Cullen, P.J.Dagnall, P.Fallon, M.J.Joyce, M.Meyer, N.Redon, P.H.Regan, J.F.Sharpey-Schafer, W.Nazarewicz, R.Wyss, Z. Phys. A 342 (1992) 371

[4] A.Kuhnert, M.A.Stoyer, J.A.Becker, E.A.Henry, M.J.Brinkman, S.W.Yates, T.F.Wang, J.A.Cizewski, F.S.Stephens, M.A.Deleplanque, R.M.Diamond, A.O.Macchiavelli, J.E.Draper, F.Azaiez, W.H.Kelly, W.Korten, Phys. Rev. C 46 (1992) 133

[5] R.M.Clark, R.Wadsworth, E.S.Paul, C.W.Beausang, I.Ali, A.Astier, D.M.Cullen, P.J.Dagnall, P.Fallon, M.J.Joyce, M.Meyer, N.Redon, P.H.Regan,W.Nazarewicz, R.Wyss, Phys. Lett. B 275 (1992) 247

[6] R.M.Clark, R.Wadsworth, E.S.Paul, C.W.Beausang, I.Ali, A.Astier, D.M.Cullen, P.J.Dagnall, P.Fallon, M.J.Joyce, M.Meyer, N.Redon, P.H.Regan, J.F.Sharpey–Schafer, W.Nazarewicz, R.Wyss, Nucl. Phys. A 562 (1993) 121

[7] T.F.Wang, E.A.Henry, J.A.Becker, A.Kuhnert, M.A.Stoyer, S.W.Yates, M.J.Brinkman, J.A.Cizewski, A.O.Macchiavelli, F.S.Stephens, M.A.Deleplanque, R.M.Diamond, J.E.Draper, F.A.Azaiez, W.H.Kelly, W.Korten, E.Rubel, Y.A.Akovali, Phys. Rev. Lett 69 (1992) 1737

[8] G.Baldsiefen, H.Hubel, B.V.Thirumala Rao, D.Mehta, U.Birkental, G.Frohlingsdorf, M.Neffgen, N.Nenoff, S.C.Pancholi, N.Singh, W.Schmitz, K.Theine, P.Willsau, H.Grawe, J.Heese, H.Kluge, K.H.Maier, M.Schramm, R.Schubart, Phys. Lett. B 275 (1992) 252

[9] G.Baldsiefen, H.Hubel, F.Azaiez, C.Bourgeois, D.Hojman, A.Korichi, N.Perrin, H.Sergolle, Z. Phys. A 343 (1992) 245

[10] J.R.Hughes et al, to be published

[11] R.M.Clark, R.Wadsworth, F.Azaiez, C.W.Beausang, A.M.Bruce, P.J.Dagnall, P.Fallon, P.M.Jones, M.J.Joyce, A.Korichi, E.S.Paul, J.F.Sharpey-Schafer, J. Phys. G 19 (1993) L57

[12] P.Dagnall et al, to be published

[13] F.Dönau and S.Frauendorf, Proc. Int. Conf. on High Angular Momentum Properties of Nuclei, Oak Ridge (1982), Nucl. Sci. Res. Conf. Series vol. 4 (Harwood, New York) p. 143

[14] S.Frauendorf in Proc. 21st Int. Symp. on Rapidly Rotating Nuclei, Tokyo (1992), Nucl Phys A 557 (1993) 259c

[15] The 8pi–Spectrometer, Proposal for a National Facility, eds H.R.Andrews, E.Hagberg, D.Horn, M.A.Lone, H.Schmeing, D.Ward, P.Taras, J.Gascon, J.C.Waddington, G.Palameta, V.Koslowsky, O.Häusser (Chalk River Laboratories, AECL–8329, 1984)

[16] T.K.Alexander and A.Bell, NIM 81 (1970) 22

[17] T.K.Alexander and J.S.Forster, Adv. Nucl. Phys. 10 (1978) 197

[18] P.J.Nolan, Nucl. Phys. A 520 (1990) 657c

[19] H.Bateman, Proc. Camb. Phil. Soc. 15 (1910) 423

[20] H.Ejiri and M.J.A.de Voigt, Gamma–Ray and Electron Spectroscopy in Nuclear Physics (Oxford: Oxford University Press) pp504

[21] Table of Isotopes, 7th edition, eds C.M.Lederer and V.S.Shirley (John Wiley and Sons Inc., New York, 1978)

[22] J.Penninga, W.H.A.Hesselink, A.Balanda, A.Stolk, H.Verheul, J. Van Klinken, H.J.Riczibos, M.J.A.De Voigt, Nucl. Phys. A 471 (1987) 535

[23] H.E.Mahnke, E.Dafni, G.D.Sprouse, T.K.Alexander, H.R.Andrews, O.Häusser, P.Taras, D.Ward, in Symp. on High Spin Phenomena in Nuclei, Argonne, ed T.L.Khoo, ANL/PHY–79–4, Argonne, (1979) 463

[24] D.J.Thouless and J.G.Valatin, Nucl. Phys. 31 (1962) 24

[25] M.Harvey and M.G.Vassanji, Nucl. Phys. A 344 (1980) 61

[26] F.Cuypers, Nucl. Phys. A 468 (1987) 237

[27] D.B.Fossan, J.R.Hughes, Y.Liang, R.Ma, E.S.Paul, N.Xu, Nucl. Phys. A 520 (1990) 214c

[28] E.S.Paul, D.B.Fossan, Y.Liang, R.Ma, N.Xu, Phys. Rev. C 40 (1989) 1255

[29] E.S.Paul, C.W.Beausang, D.B.Fossan, R.Ma, W.F.Piel, N.Xu, L.Hildingsson, G.A.Leander, Phys. Rev. Lett 58 (1987) 984

[30] E.S.Paul, D.B.Fossan, Y.Liang, R.Ma, N.Xu, R.Wadsworth, I.Jenkins, P.J.Nolan, Phys. Rev. C 41 (1990) 1576

Figure Captions:

Fig 1a: Partial gated spectra for the 279 and 216 keV transitions of band 3 in ^{198}Pb. The spectra were formed by summing gates above the transition of interest. The variation of the shifted, S, and unshifted, U, components of the γ–ray line, as the target–stopper separation increases, can be seen.

Fig 1b: Same as Fig. 1a, showing partial gated spectra for the 294 and 270 keV transitions of the irregular band seen in ^{197}Pb.

Fig 2a: Data showing the variation of $R(=I_U/(I_U+I_S))$ as a function of target–stopper separation, d. The solid curves represent the best fits of the data for the 279 and 216 keV transitions in band 3 of ^{198}Pb (see Fig. 1a). See text for details of the fitting procedure. The intrinsic lifetimes extracted were found to be τ_{279} ~2.1(5) ps and τ_{216} ~1.8(5) ps.

Fig 2b: Same as Fig. 2a, showing decay curves for the 294 and 270 keV transitions in the irregular band of ^{197}Pb (see Fig. 1b). The intrinsic lifetimes extracted were found to be τ_{294} ~1.3(3) ps and τ_{270} ~2.8(4) ps.

Fig 3: Partial level scheme for ^{198}Pb. Shown are bands 1 and 3, and sequences A and B, as described in [6].

Fig 4: Partial level schemes for the irregular, I, and regular, R, bands seen in ^{197}Pb [3, 4]. Note that the two bands are not drawn to the same energy scale.

Fig 5: Plot of the deduced B(M1)–values versus γ–ray energy for transitions in the four dipole sequences described in the text.

Fig 6: Schematic showing the composition and generation of angular momentum in the TAC scenario for the configurations described in the text. I_{tot} is the total angular momentum (with projections I_1 and I_3), whilst i_π and i_ν are the components resulting from the protons and neutrons, respectively.

Table 1: Measured lifetimes, τ (ps), branching ratios, B_γ, and reduced transition strengths, B(M1) (Wu), of states in ^{197}Pb and ^{198}Pb. The third column indicates the lifetime experiment. DSAM results came from [7], whilst RDM results are from the present study. All the branching ratios, used to calculate B(M1)-values, are from the EUROGAM data. A dash in that column indicates that no associated E2-crossover transition could be identified. The 207 keV transition of band 1 in ^{198}Pb is marked with an asterisk since it is a doublet and the lifetime extracted will have a contribution from both γ-ray components.

	E_γ (keV)	Expt	τ (ps)	B_γ	B(M1) (Wu)
Band 3	476	DSAM	0.27(7)	0.77(2)	$0.74^{+0.34}_{-0.14}$
^{198}Pb	472	DSAM	0.22(6)	0.84(2)	$0.99^{+0.49}_{-0.19}$
	445	DSAM	0.24(4)	0.87(2)	$1.07^{+0.38}_{-0.17}$
	423	DSAM	0.46(10)	0.88(2)	$0.69^{+0.26}_{-0.12}$
	390	DSAM	0.72(10)	0.91(2)	$0.55^{+0.11}_{-0.08}$
	343	DSAM	1.14(23)	0.89(2)	$0.48^{+0.11}_{-0.08}$
	279	RDM	2.1(5)	-	$0.45^{+0.12}_{-0.09}$
	216	RDM	1.8(5)	-	$0.83^{+0.32}_{-0.18}$
	156	RDM	2.7(9)	-	$0.67^{+0.34}_{-0.17}$
B ^{198}Pb	322	RDM	>8	-	-
	264	RDM	>4	-	-
	532	RDM	>4	-	-
Band 1	506	DSAM	0.052(11)	0.86(2)	$3.7^{+1.1}_{-0.9}$
^{198}Pb	464	DSAM	0.099(25)	0.91(2)	$2.6^{+0.9}_{-0.5}$
	422	DSAM	0.20(4)	0.90(2)	$1.6^{+0.5}_{-0.3}$
	375	DSAM	0.36(10)	0.91(2)	$1.2^{+0.5}_{-0.3}$
	326	DSAM	0.58(15)	0.95(2)	$1.1^{+0.5}_{-0.3}$
	280	RDM	1.1(6)	-	$0.8^{+1.0}_{-0.3}$
	238	RDM	0.85(30)	-	$1.5^{+0.8}_{-0.4}$
	207*	RDM	2.1(4)*	-	$0.75^{+0.18}_{-0.12}$*
A ^{198}Pb	429	RDM	3.5(15)	-	-
	228	RDM	4.6(14)	-	-
Regular	267	RDM	1.2(3)	-	$1.01^{+0.87}_{-0.29}$
^{197}Pb	201	RDM	0.9(4)	-	$2.08^{+1.25}_{-0.57}$
	151	RDM	1.8(8)	-	$1.32^{+1.32}_{-0.44}$
Irregular	294	RDM	1.3(3)	0.90(2)	$0.59^{+0.17}_{-0.12}$
^{197}Pb	365	RDM	1.3(3)	0.85(2)	$0.34^{+0.11}_{-0.08}$
	385	RDM	1.1(3)	0.87(2)	$0.35^{+0.14}_{-0.08}$
	370	RDM	1.3(3)	0.89(2)	$0.34^{+0.11}_{-0.07}$
	359	RDM	1.3(3)	0.92(2)	$0.38^{+0.11}_{-0.08}$
	270	RDM	2.8(4)	-	$0.31^{+0.06}_{-0.05}$
	152	RDM	3.1(7)	-	$0.76^{+0.22}_{-0.14}$

Table 2: B(M1)/B(E2) values measured from the EUROGAM data (see text).

Structure	M1 (keV)	E2 (keV)	Measured B(M1)/B(E2) $(\mu_N/eb)^2$
Band 1 ^{198}Pb	592	1142	21(3)
	550	1056	30(3)
	506	970	27(3)
	464	886	34(3)
	422	797	26(3)
	375	701	21(2)
	326	607	32(3)
Band 3 ^{198}Pb	476	948	17(2)
	472	917	23(2)
	444	867	25(3)
	423	812	24(2)
	389	732	26(3)
	343	622	13(4)
Irregular ^{197}Pb	327	572	23(9)
	245	530	23(6)
	285	513	20(6)
	228	522	26(7)
	294	659	28(4)
	365	750	15(2)
	385	755	15(2)
	370	729	23(3)
	359	629	17(4)
Regular ^{197}Pb	467	913	32(5)
	446	850	17(3)
	404	741	24(4)

Table 3: The proposed configurations from [6] for the bands in ^{197,198}Pb. The neutron configurations in an unpaired scheme are given in terms of the occupation of states relative to the N=120 oblate subshell closure. The neutron configuration of the irregular band in ^{197}Pb was not assigned and is labelled νX in the table.

Structure	Nucleus	Configuration
Band 1	^{198}Pb	$\pi(h_{9/2}\otimes i_{13/2})\otimes\nu 6^{-4}$
Band 3	^{198}Pb	$\pi(h_{9/2})^2 \otimes \nu 6^{-3}5^{-1}$
Regular	^{197}Pb	$\pi(h_{9/2}\otimes i_{13/2})\otimes\nu 6^{-3}5^{-2}$
Irregular	^{197}Pb	$\pi(h_{9/2}\otimes s_{1/2})\otimes\nu X$

Table 4: Deduced B(E2) transition rates (in e^2b^2) for bands 1 and 3 in ^{198}Pb and the irregular band in ^{197}Pb. Also given are the corresponding quadrupole moments and β_2 values.

Structure	E_γ(keV)	B_γ	B(E2) $(eb)^2$	Q_0 (eb)	β_2
Band 1	970	0.14(2)	$0.24^{+0.06}_{-0.04}$	$2.32^{+0.27}_{-0.20}$	$0.076^{+0.009}_{-0.006}$
^{198}Pb	886	0.09(2)	$0.14^{+0.05}_{-0.03}$	$1.77^{+0.29}_{-0.20}$	$0.059^{+0.010}_{-0.006}$
	797	0.10(2)	$0.11^{+0.03}_{-0.02}$	$1.57^{+0.20}_{-0.15}$	$0.052^{+0.006}_{-0.005}$
	701	0.09(2)	$0.12^{+0.05}_{-0.03}$	$1.64^{+0.31}_{-0.22}$	$0.054^{+0.010}_{-0.007}$
	607	0.05(2)	$0.10^{+0.03}_{-0.02}$	$1.50^{+0.21}_{-0.16}$	$0.049^{+0.007}_{-0.005}$
Band 3	948	0.23(2)	$0.091^{+0.032}_{-0.019}$	$1.43^{+0.23}_{-0.16}$	$0.047^{+0.008}_{-0.005}$
^{198}Pb	917	0.16(2)	$0.092^{+0.035}_{-0.020}$	$1.44^{+0.25}_{-0.17}$	$0.047^{+0.008}_{-0.006}$
	867	0.13(2)	$0.090^{+0.018}_{-0.013}$	$1.42^{+0.14}_{-0.11}$	$0.047^{+0.004}_{-0.004}$
	812	0.12(2)	$0.060^{+0.017}_{-0.011}$	$1.16^{+0.15}_{-0.11}$	$0.038^{+0.005}_{-0.004}$
	732	0.09(2)	$0.051^{+0.008}_{-0.006}$	$1.07^{+0.08}_{-0.07}$	$0.035^{+0.003}_{-0.002}$
	622	0.11(2)	$0.085^{+0.021}_{-0.015}$	$1.38^{+0.16}_{-0.13}$	$0.045^{+0.006}_{-0.004}$
Irregular	659	0.10(2)	$0.050^{+0.015}_{-0.010}$	$1.06^{+0.15}_{-0.11}$	$0.035^{+0.005}_{-0.004}$
^{197}Pb	750	0.15(2)	$0.040^{+0.012}_{-0.007}$	$0.95^{+0.13}_{-0.09}$	$0.031^{+0.005}_{-0.004}$
	755	0.13(2)	$0.039^{+0.015}_{-0.008}$	$0.94^{+0.16}_{-0.11}$	$0.031^{+0.005}_{-0.004}$
	729	0.11(2)	$0.034^{+0.010}_{-0.006}$	$0.87^{+0.12}_{-0.08}$	$0.029^{+0.004}_{-0.003}$
	629	0.08(2)	$0.051^{+0.015}_{-0.010}$	$1.07^{+0.15}_{-0.11}$	$0.035^{+0.006}_{-0.004}$

Table 5: Calculated B(M1) transition rates (in Wu) for the various proton configurations coupled to different numbers of $i_{13/2}$ (N=6) neutrons. The calculations were performed using the semi-classical Dönau and Frauendorf formula [13].

		ν			
		0	6^1	6^2	6^3
	$h_{9/2}\otimes i_{13/2}$	1.97	3.48	5.06	6.54
π	$h^2_{9/2}$	0.44	1.01	1.64	2.80
	$h_{9/2}\otimes s_{1/2}$	0.56	0.92	1.28	1.90

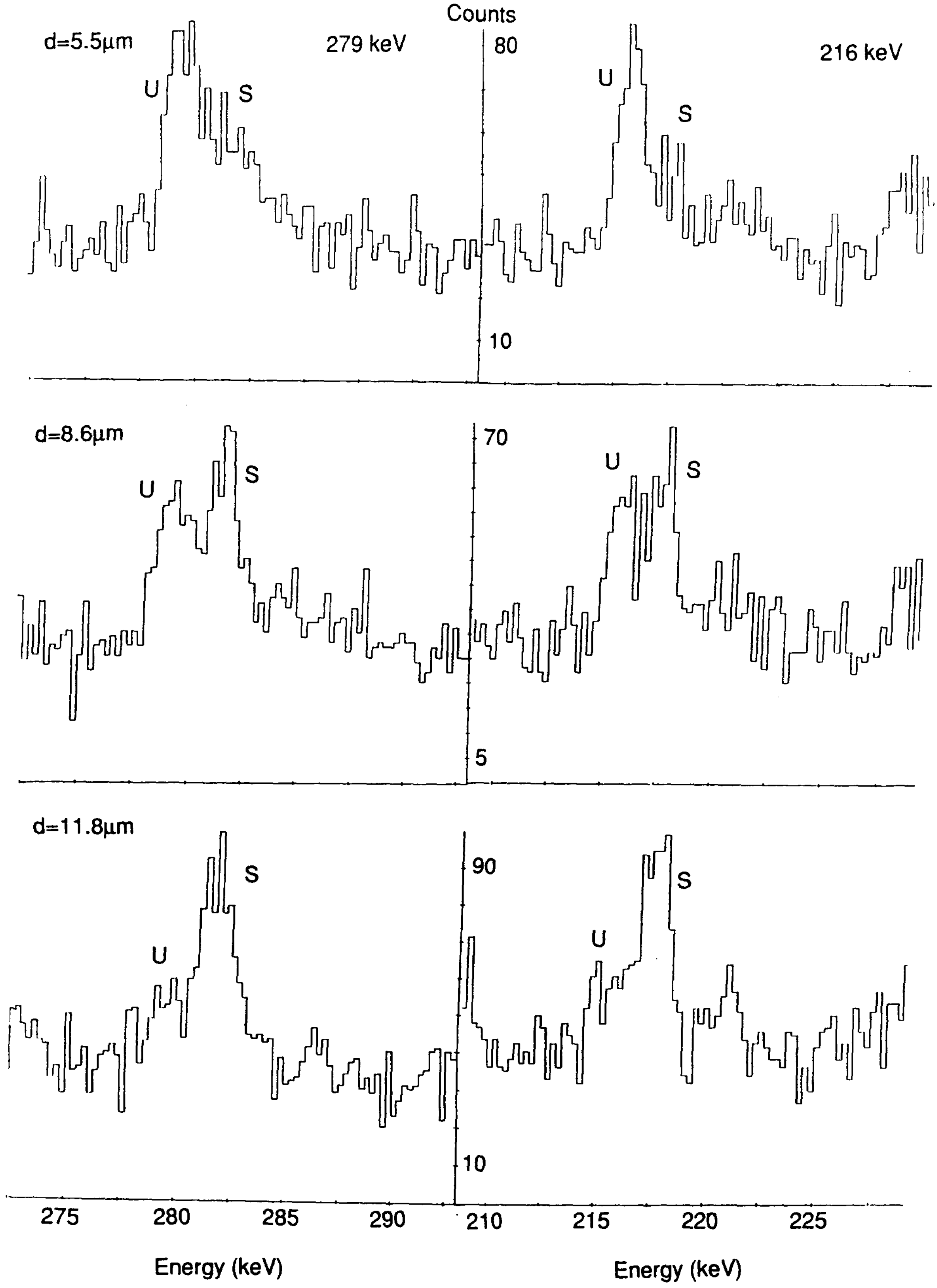

Counts
d=5.5μm
279 keV
80
216 keV
U
S
U
S
10
d=8.6μm
70
U
S
U
S
5
d=11.8μm
90
S
S
U
U
10
275
280
285
290
210
215
220
225
Energy (keV)
Energy (keV)

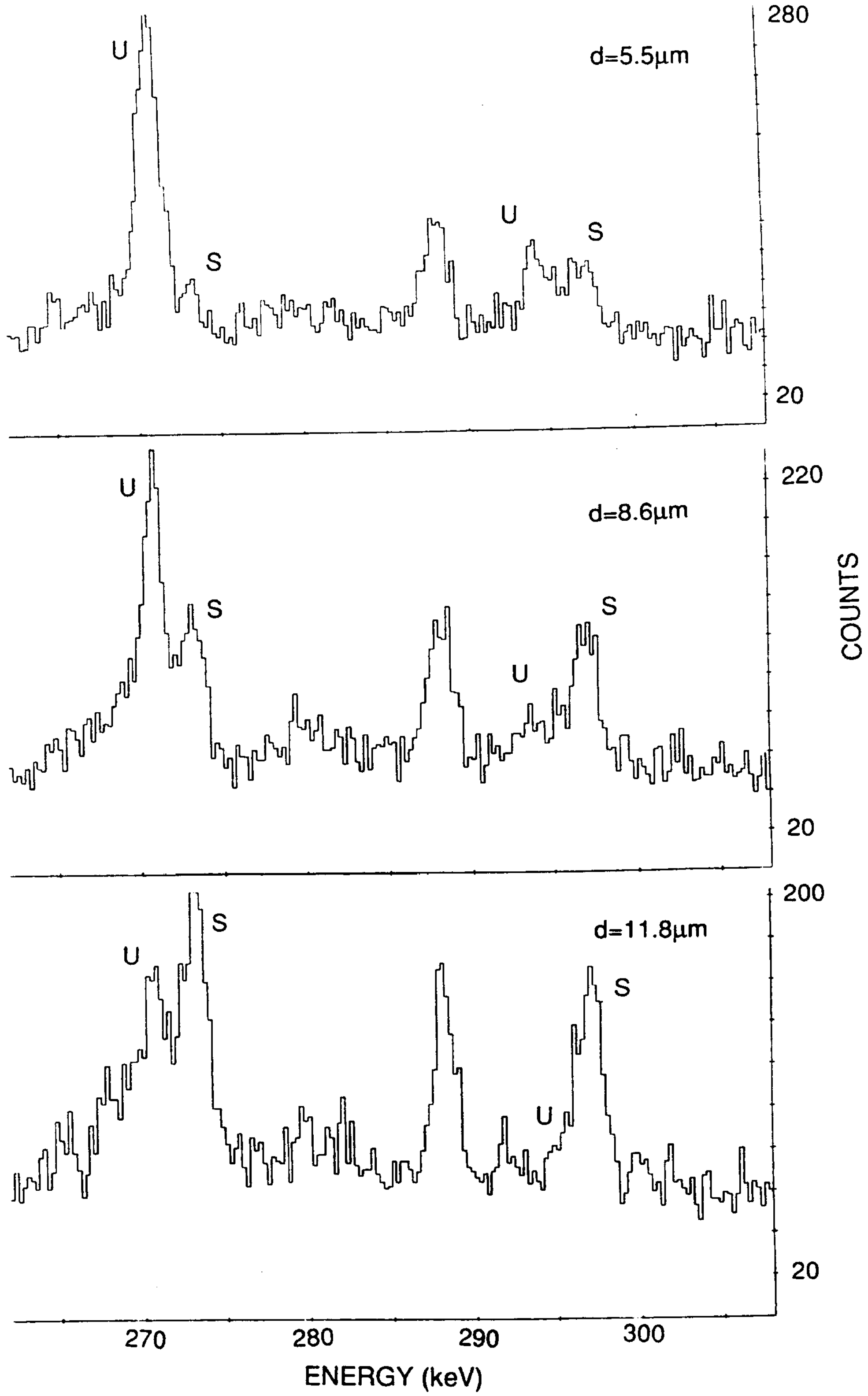

280
d=5.5μm
U
S
U
S
20
220
d=8.6μm
U
S
S
U
20
COUNTS
200
d=11.8μm
S
U
S
U
20
270
280
290
300
ENERGY (keV)

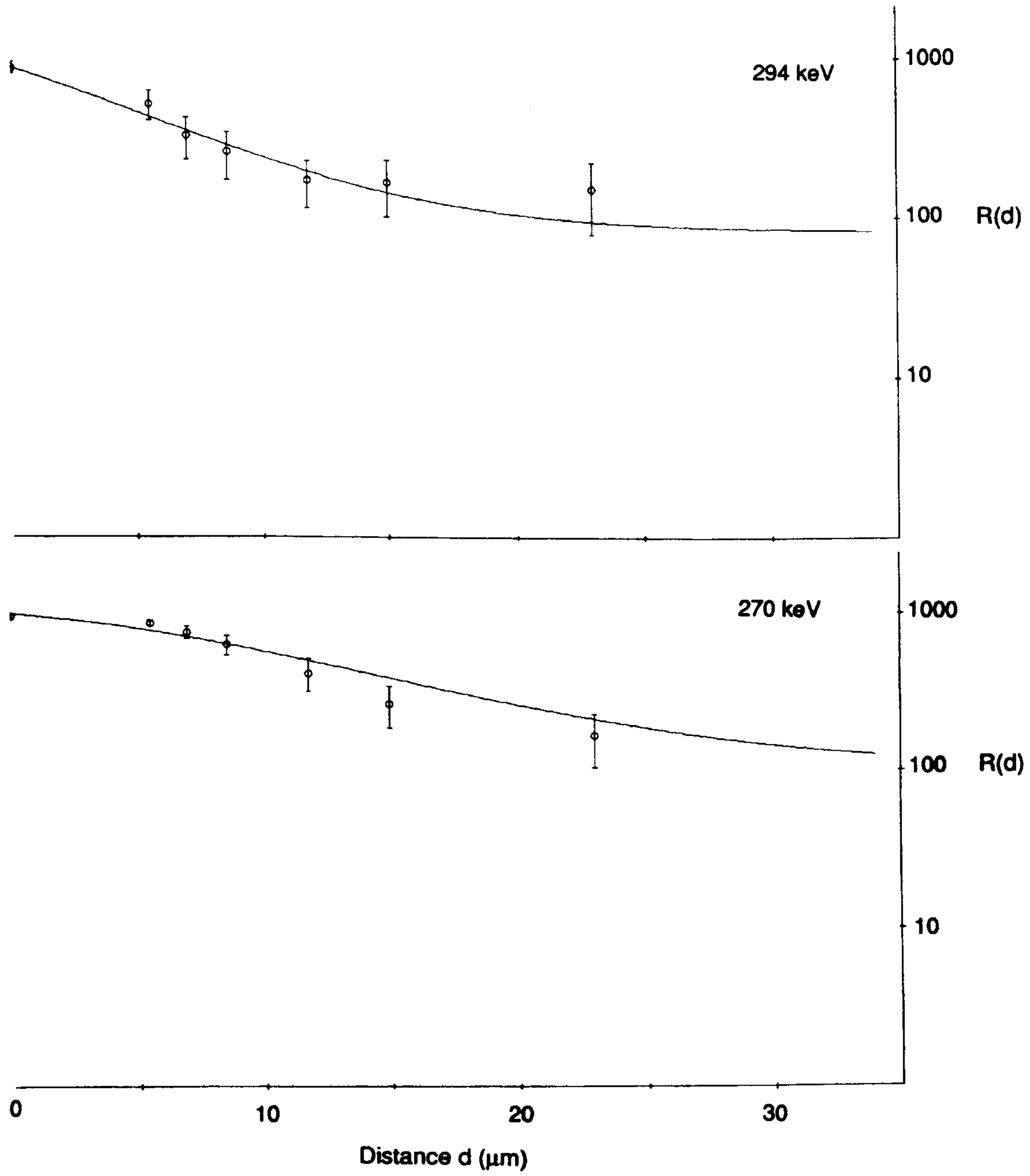

294 keV
1000
100
R(d)
10
270 keV
1000
100
R(d)
10
0
10
20
30
Distance d (μm)

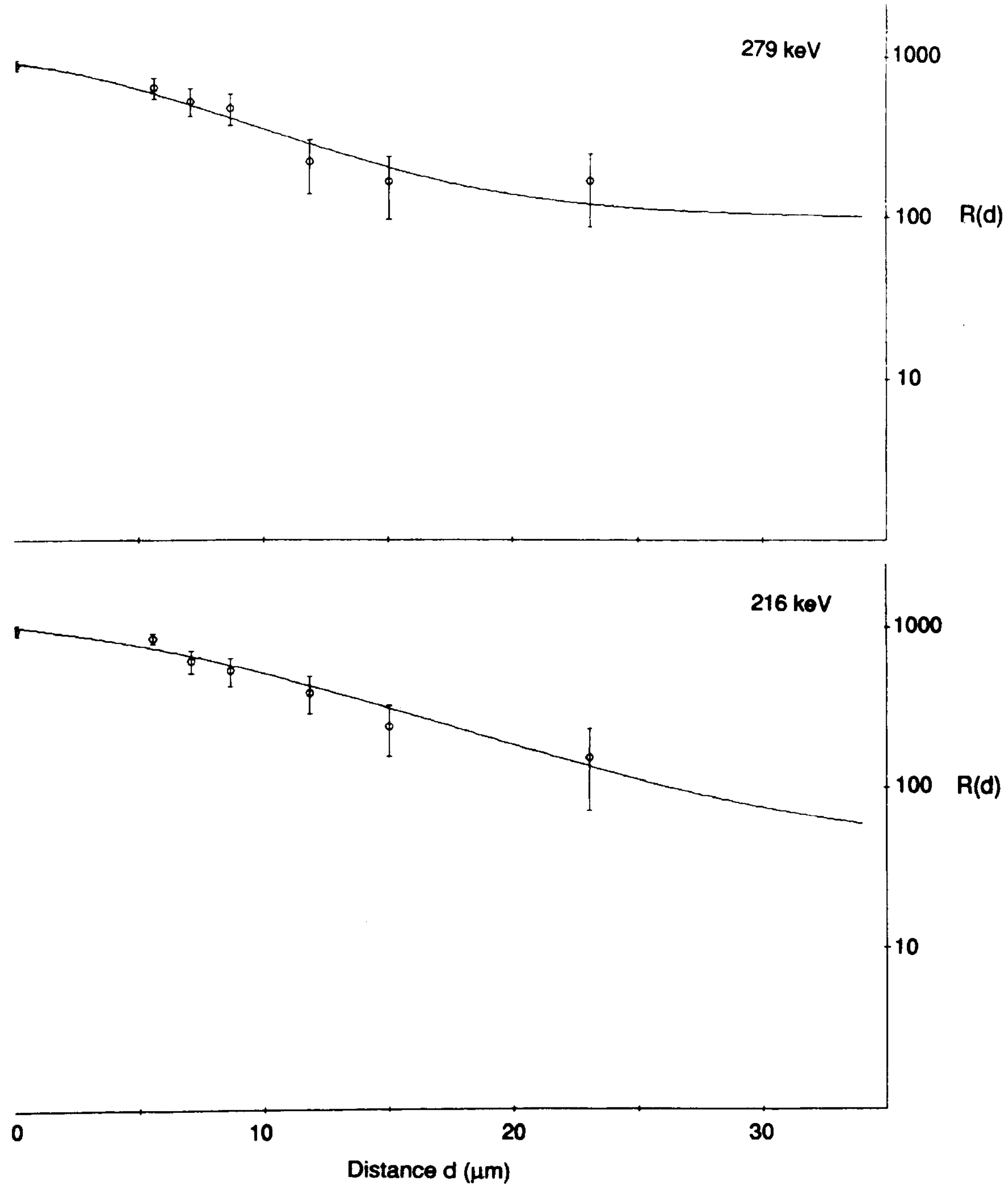
279 keV
1000
100
10
R(d)
216 keV
1000
100
10
R(d)
0
10
20
30
Distance d (μm)

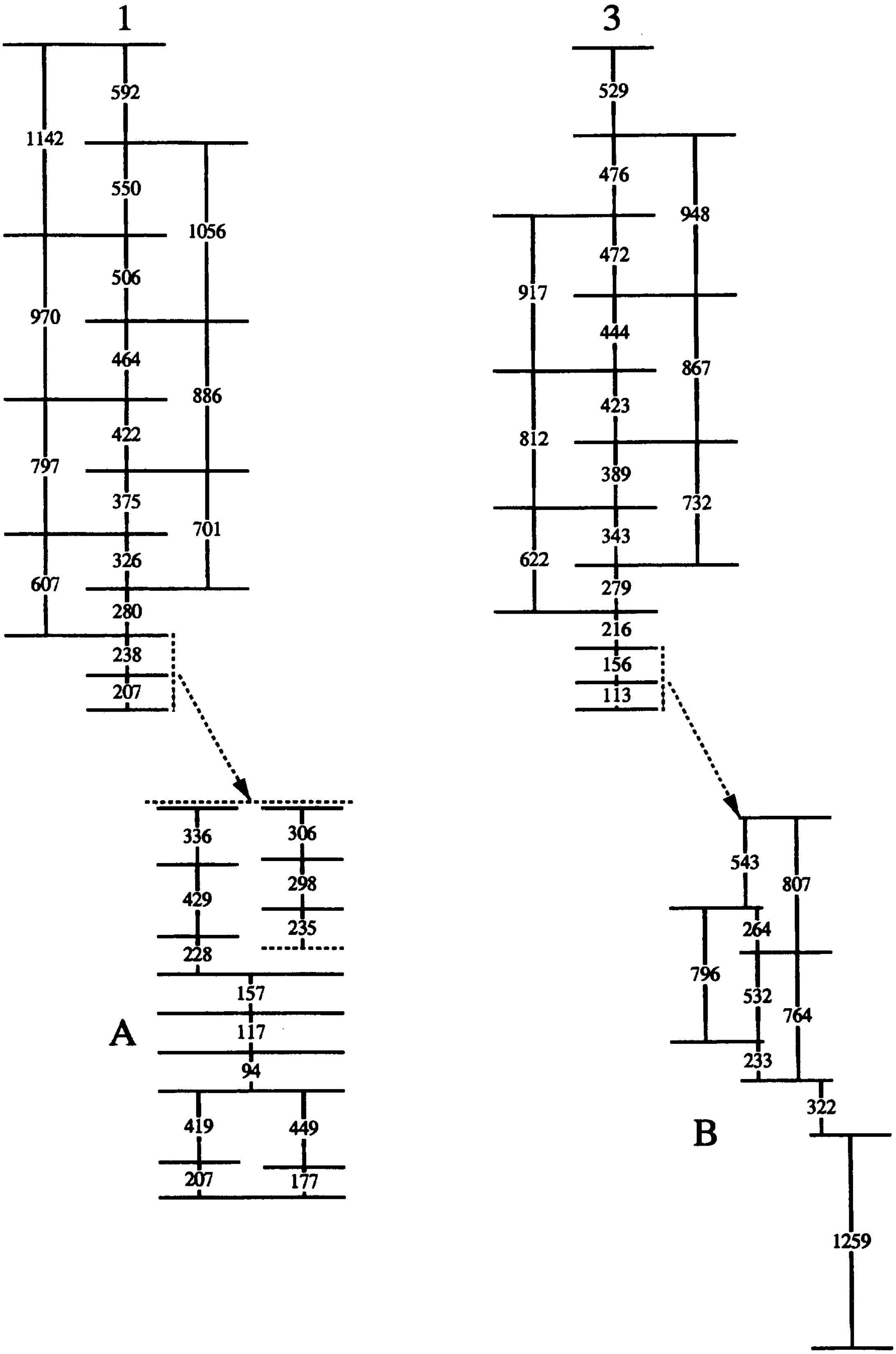
1
592
1142
550
1056
506
970
464
886
422
797
375
701
326
607
280
238
207
336
306
429
298
235
228
157
A
117
94
419
449
207
177
3
529
476
948
472
917
444
867
423
812
389
732
343
622
279
216
156
113
543
807
264
796
532
764
233
322
B
1259

^{198}Pb

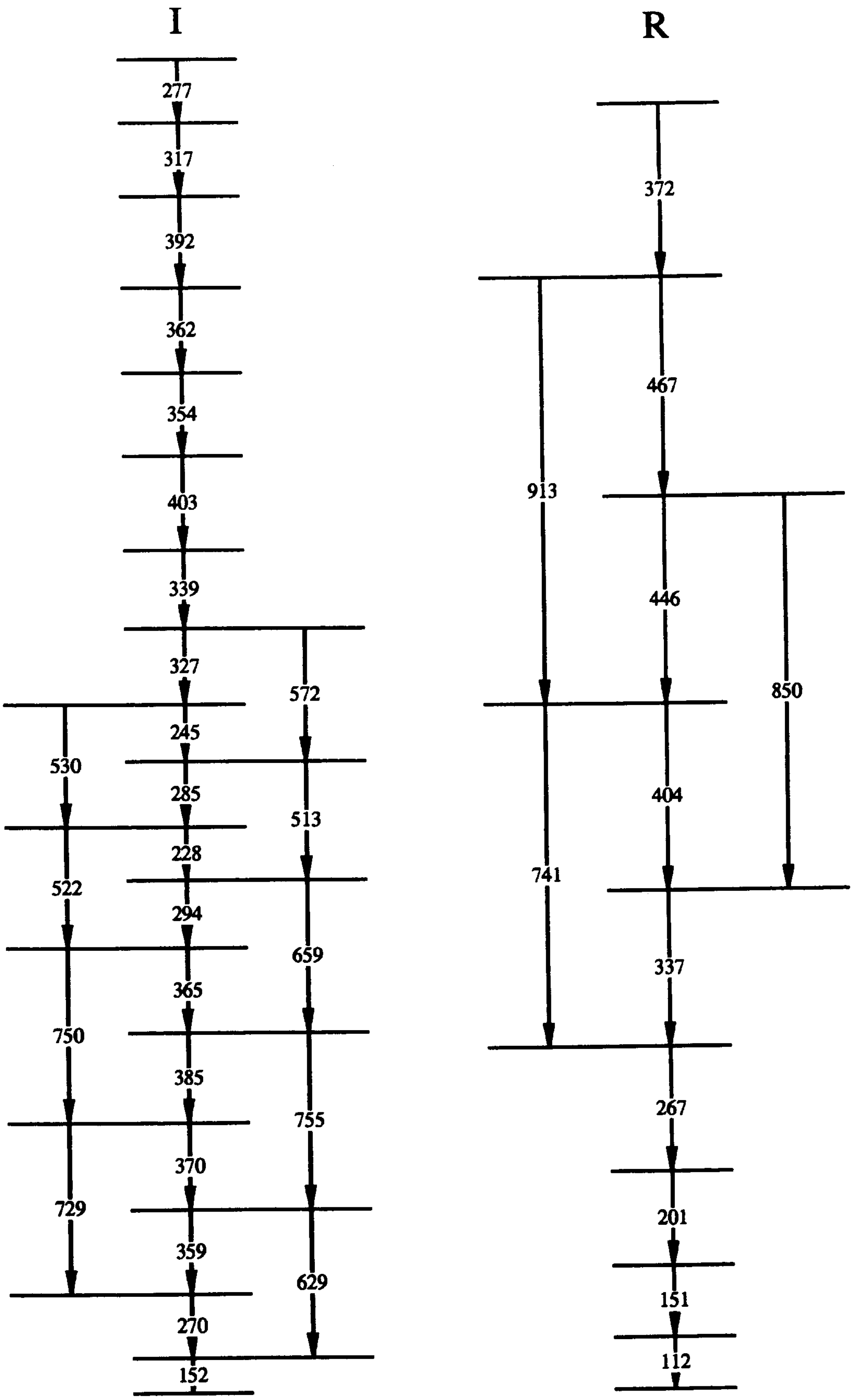
I
R
277
317
392
362
354
403
339
327
572
245
530
285
513
228
522
294
659
365
750
385
755
370
729
359
629
270
152
372
467
913
446
850
404
741
337
267
201
151
112

^{197}Pb

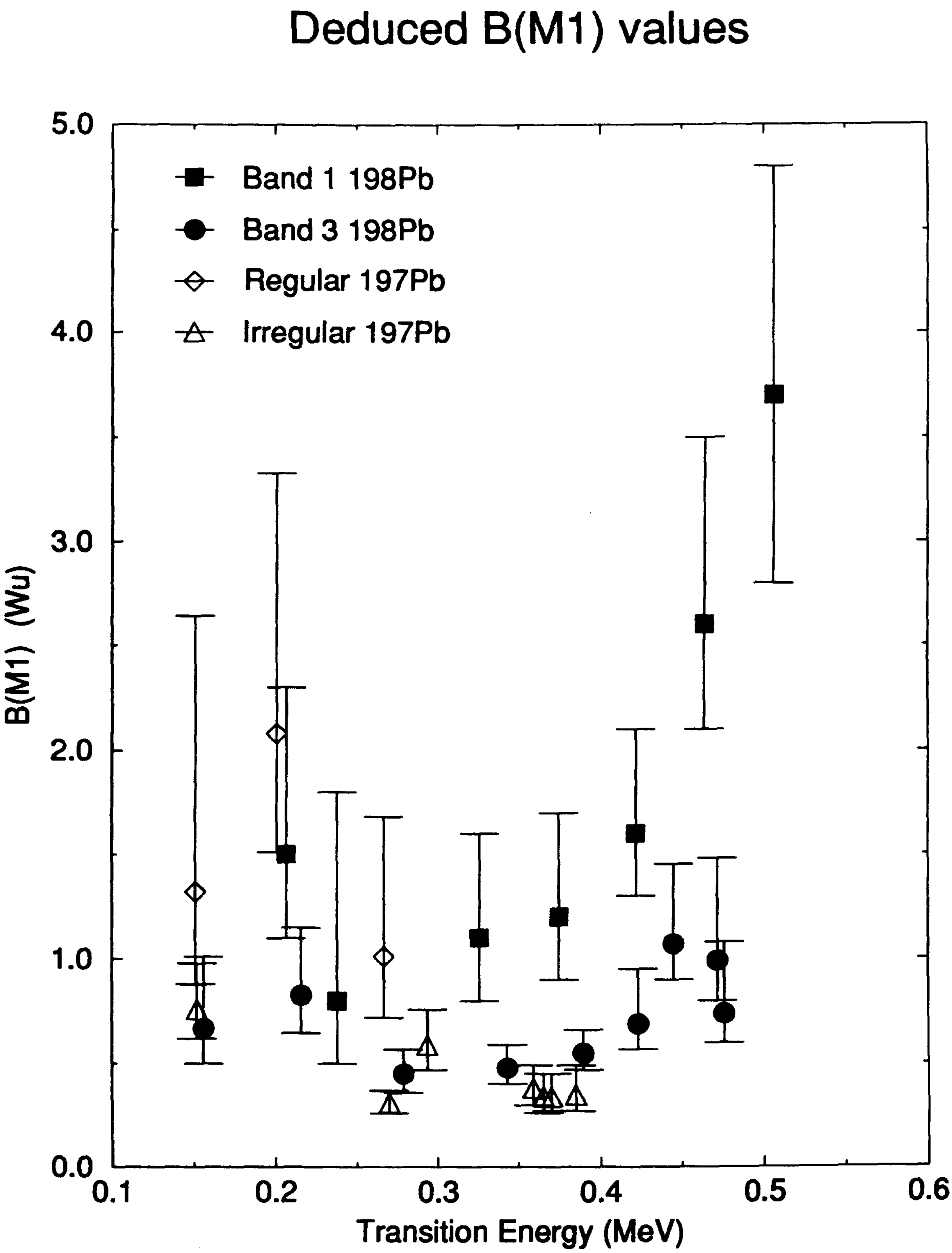
Deduced B(M1) values
Band 1 198Pb
Band 3 198Pb
Regular 197Pb
Irregular 197Pb
B(M1) (Wu)
Transition Energy (MeV)
5.0
4.0
3.0
2.0
1.0
0.0
0.1
0.2
0.3
0.4
0.5
0.6

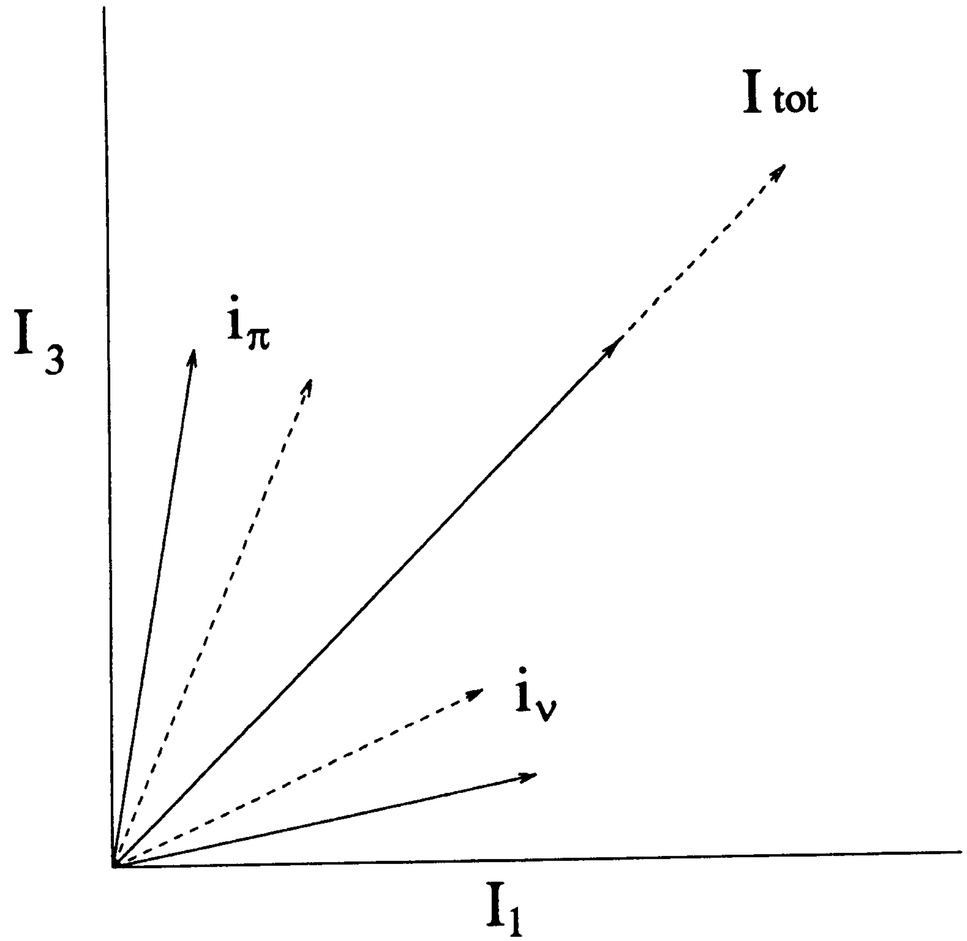

I_3
i_π
I_{tot}
i_ν
I_1